Journal of Loss Prevention in the Process Industries 67 (2020) 104231

Contents lists available at ScienceDirect

Journal of Loss Prevention in the Process Industries

journal homepage: http://www.elsevier.com/locate/jlp

CFD Simulation of the Dispersion of Binary Dust Mixtures in the 20 L Vessel

Maria Portarapillo [a], Valeria Di Sarli [b], Roberto Sanchirico [b], Almerinda Di Benedetto [a,*]

[a] Dipartimento di Ingegneria Chimica, dei Materiali e della Produzione Industriale, Università degli Studi di Napoli Federico II, Piazzale Tecchio 80, 80125, Napoli, Italy
[b] Istituto di Ricerche sulla Combustione, Consiglio Nazionale delle Ricerche (CNR), Piazzale Tecchio 80, 80125, Napoli, Italy

ARTICLE INFO

Keywords:
CFD simulation
Dust mixtures
Dust dispersion
Dust density
Dust diameter
Siwek sphere

ABSTRACT

There are at least two main requirements for repeatable and reliable measurements of flammability and explosibility parameters of dusts: a uniform dispersion of solid particles inside the test vessel, and a homogeneous degree of turbulence. In several literature works, it has been shown that, in the standard 20 L sphere, the dust injection system generates a non-uniform dust cloud, while high gradients characterize the turbulent flow field. In this work, the dust dispersion inside the 20 L sphere was simulated for nicotinic acid/anthraquinone mixtures (with different pure dust ratios, while keeping the total dust concentration constant) with a validated three-dimensional CFD model. Numerical results show that the fields of dust concentration, flow velocity and turbulence are strongly affected by both diameter and density of the pure dusts. These different dust properties lead to segregation phenomena with the formation of zones richer in one component and leaner in the other one and *vice versa*, and also result in preferential paths for the solid particles inside the sphere. Overall, the obtained results highlight the need for developing a dust injection system able to overcome the shortcomings of the actual one even when testing dust mixtures.

1. Introduction

In food, pharmaceutical and wood industries and chemical manufacturing, a high number of accidents are imputable to explosions of flammable dusts, dust mixtures, and hybrid mixtures. Prevention and protection measures from accidental explosions are based on the knowledge of the main parameters that characterize their flammability and explosibility.

The flammability parameters are the Minimum Ignition Energy (MIE), the Minimum Ignition Temperature (MIT), the Minimum Explosible Concentration (MEC), and the Limiting Oxygen Concentration (LOC). Recently, a new flammability parameter has been proposed, the so-called Volatile Point (VP) (Sanchirico et al., 2018).

The explosion parameters are derived from the pressure-time profile recorded when the flammable dust, dust mixture, or hybrid mixture explodes in air under near adiabatic conditions. They are the maximum explosion pressure (P_{MAX}) and the deflagration index ($K_{St} = (dP/dt)_{max} \cdot V^{1/3}$). The deflagration index quantifies the explosion severity and its knowledge allows for hazard classification.

Standard procedures and equipment for measurement of dust flammability and explosibility parameters are defined by international standards (Zalosh, 2019). The experimental devices available at our laboratory fulfill the ASTM standard (deflagration index and maximum pressure (ASTM E1226-19, 2019); minimum ignition temperature (ASTM E1491-06, 1991); minimum ignition energy (ASTM E2019-03, 1999); minimum explosible concentration (ASTM E1515-14, 1993); layer ignition temperature (ASTM E2021-15, 1999); limiting oxygen concentration (ASTM E2931-13, 2013); flash point (ASTM E502-07, 1984)). According to these procedures, the evaluation of MEC, LOC, P_{MAX} and K_{St} for dust-air, dust mixture-air and dust/gas mixture-air is performed in a standard explosion apparatus that consists of a closed steel combustion chamber with an internal volume of at least 20 L, spherical or cylindrical (with a length-to-diameter ratio of approximately 1:1) in shape. Two major requirements for the apparatus are the ability of dispersing a fairly uniform dust cloud in the vessel and the ability of realizing a controlled turbulence level. According to the standard procedure (ASTM E1226-19, 2019), the dust sample is loaded in the dust container together with compressed air (21 bar). The sphere is initially pre-evacuated at 0.4 bar. When the valve connecting the container to the sphere is opened, the dust is injected into the sphere. At the bottom of the vessel, a rebound nozzle is placed to allow dispersion of the dust-air mixture inside the vessel. When the valve is opened, the pressure difference between the container loaded with dust and the sphere generates turbulence which decays in time. The dust-air mixture

* Corresponding author.
E-mail address: almerinda.dibenedetto@unina.it (A. Di Benedetto).

https://doi.org/10.1016/j.jlp.2020.104231
Received 15 April 2020; Received in revised form 6 July 2020; Accepted 9 July 2020
Available online 19 July 2020

Table 1
Simulation conditions.

Parameter	Value
Dust container volume (L)	0.6
Sphere volume (L)	20
Initial pressure of the container (bar)	21
Initial pressure of the sphere (bar)	0.4
Dust concentration (g/m^3)	250

Table 2
Dust properties used for simulation.

Property	Niacin	Anthraquinone
Density (kg/m^3)	1470	1310
Diameter (μm)	41.4	26.9

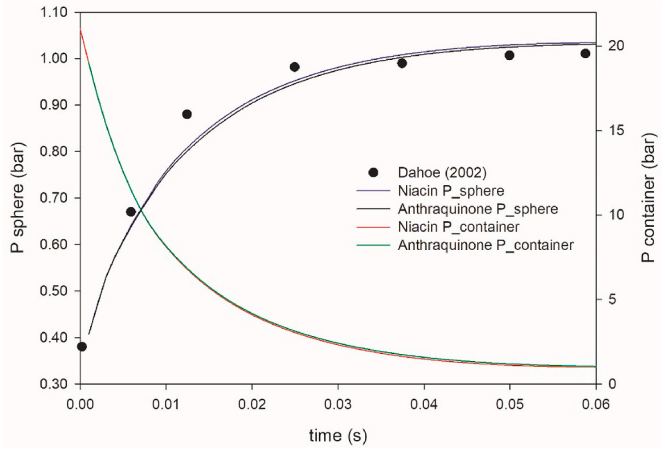

Fig. 1. Pressure-time profiles computed in the sphere and in the container for pure dusts, and literature data for the sphere (Dahoe et al., 2002).

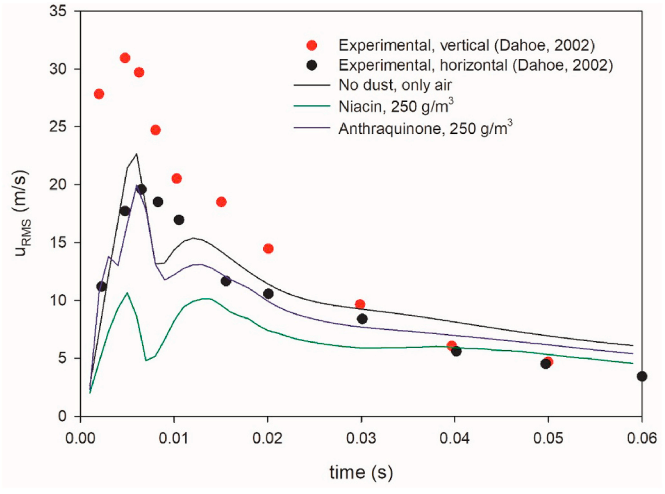

Fig. 2. Temporal trends of root mean square velocity for only air, niacin and anthraquinone: simulations and literature data (these latter are for only air) (Dahoe et al., 2002).

passes through the holes and, following the shape of the profiles of the rebound nozzle, is dispersed inside the sphere, thus creating the dust-air cloud.

Literature studies have shown that the standard procedure suffers from issues related to the control of the turbulence level and to the ability of generating a uniform cloud. The turbulence level generated inside the sphere varies in time, space and with the dust properties (Dahoe et al., 2002; Hauert and Vogl, 1995; Pu et al., 1991; van der Wel et al., 1992). Di Benedetto and co-workers have shown that, with the standard procedure/equipment, it is not possible to generate uniform dust dispersion and turbulence inside the sphere (Di Benedetto et al., 2013). In particular, the turbulence level and the dust particle distribution inside the 20 L sphere significantly depend on the dust size (Di Benedetto et al., 2010; Di Sarli et al., 2013; Russo et al., 2013), concentration (Di Sarli et al., 2014) and shape (Russo and Di Benedetto, 2013).

In the case of dust mixtures with different properties (size, density and shape) of the pure components, these issues may become especially critical for the correct evaluation of safety parameters (Sanchirico et al., 2015b). In addition, it has also been shown that the particle size, which is a fundamental parameter affecting the spatio-temporal evolution of explosion pressure, can be greatly reduced during the dispersion process due to the passage through the holes of the rebound nozzle (Sanchirico et al., 2015a).

In this work, we aim at investigating the dust dispersion and turbulence generation in the 20 L sphere for the case of dust mixtures. To this end, simulations for nicotinic acid/anthraquinone mixtures were performed with a validated three-dimensional CFD model.

2. Model description

Niacin (nicotinic acid, $C_6H_5NO_2$) is an organic compound classified as a B-vitamin. It is used mainly in the pharmaceutical industry, and it is also a reference dust for testing dust explosion. Anthraquinone (9,10-dioxoanthracene, $C_{14}H_8O_2$) is an aromatic compound. It is used in the production of dyes and natural pigments, as a catalyst in the production of wood pulp in the paper industry, and as a laxative in the pharmaceutical industry. These two dusts were chosen since, in recent investigations, it has been found the occurrence of synergistic effects between niacin and anthraquinone that affect the flammability and explosibility parameters (Centrella et al., 2020; Portarapillo et al., 2020; Sanchirico et al., 2018).

Detailed model description was given in a previous paper (Di Benedetto et al., 2013). The model consists of the time-averaged Navier--Stokes equations (Eulerian approach) written in polar coordinates. Turbulence was modelled using the standard k-ε closure (Launder and Spalding, 1972). The flow of the solid phase was solved with the Lagrangian approach using the discrete phase model (DPM). The interaction between the fluid phase and the solid particles was found to be a two-way coupling according to the classification proposed by Elghobashi (1994). Thus, the interaction between dust particles was fully neglected.

In previous works, the model was validated versus experimental data (Di Benedetto et al., 2013; Di Sarli et al., 2015) and used to simulate turbulent flow field and dust dispersion inside the 20 L sphere equipped with the rebound nozzle (Di Benedetto et al., 2013; Di Sarli et al., 2014, 2013), the perforated annular nozzle (Di Sarli et al., 2015), and one fan/two fans (Di Benedetto et al., 2015).

The fluid flow equations were discretized using a finite-volume formulation on a three-dimensional non-uniform unstructured grid. The spatial discretization of the model equations used first-order schemes for convective terms and second-order schemes for diffusion terms. First-order time integration was used to discretize temporal derivatives with a time step of $1 \cdot 10^{-4}$ s.

The discrete phase model is described by ordinary differential equations. Therefore, the DPM uses its own numerical mechanisms and discretization schemes. For particle tracking, we used an automated scheme that provides a mechanism to switch in an automated fashion between numerically stable lower-order schemes and higher-order schemes, which are stable only in a limited range. The particle tracking integration time step was taken equal to the fluid flow time step

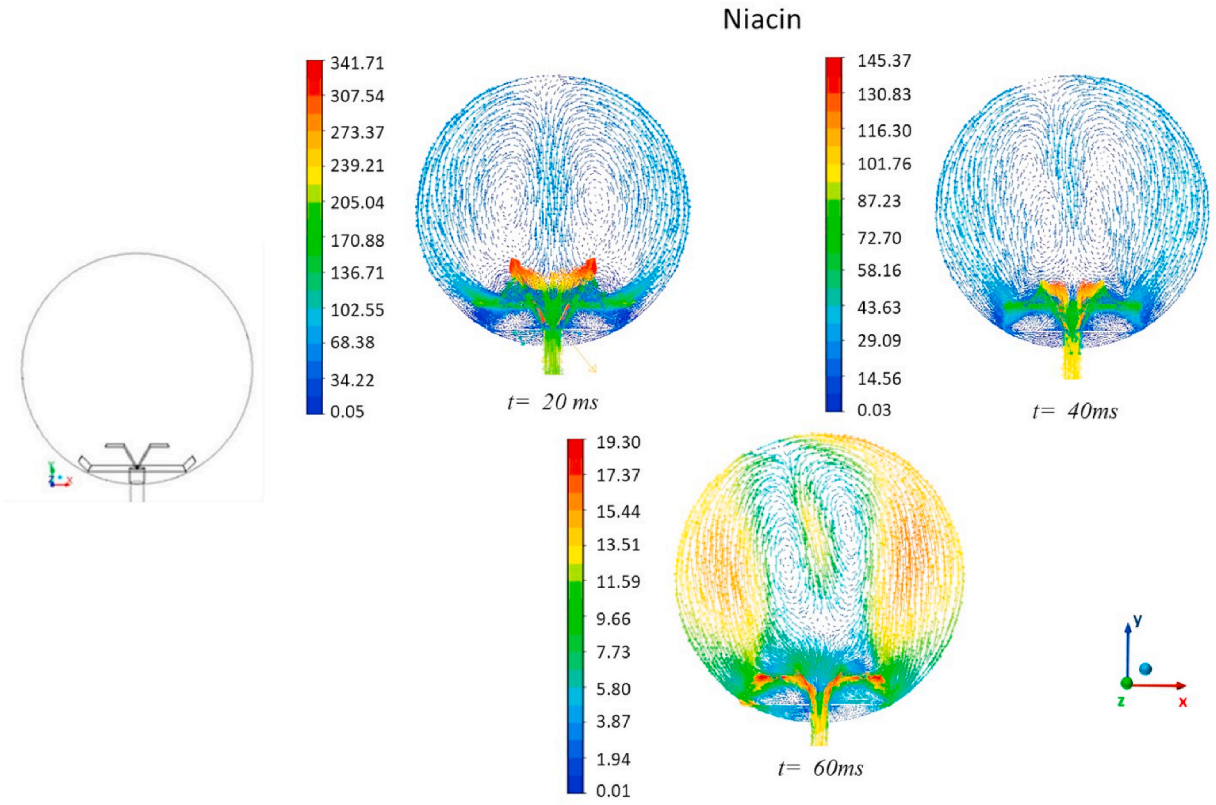

Fig. 3. Time sequence of maps of velocity vectors colored by velocity magnitude (m/s): niacin (frontal view).

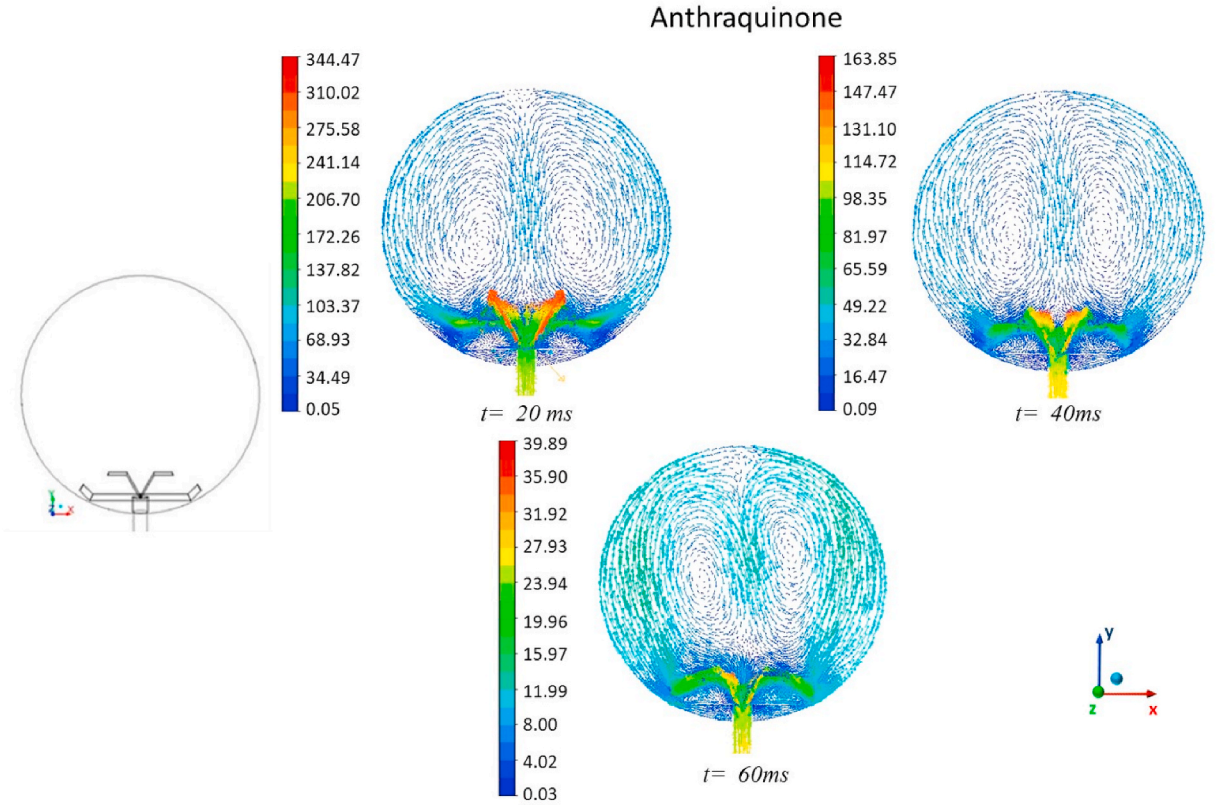

Fig. 4. Time sequence of maps of velocity vectors colored by velocity magnitude (m/s): anthraquinone (frontal view).

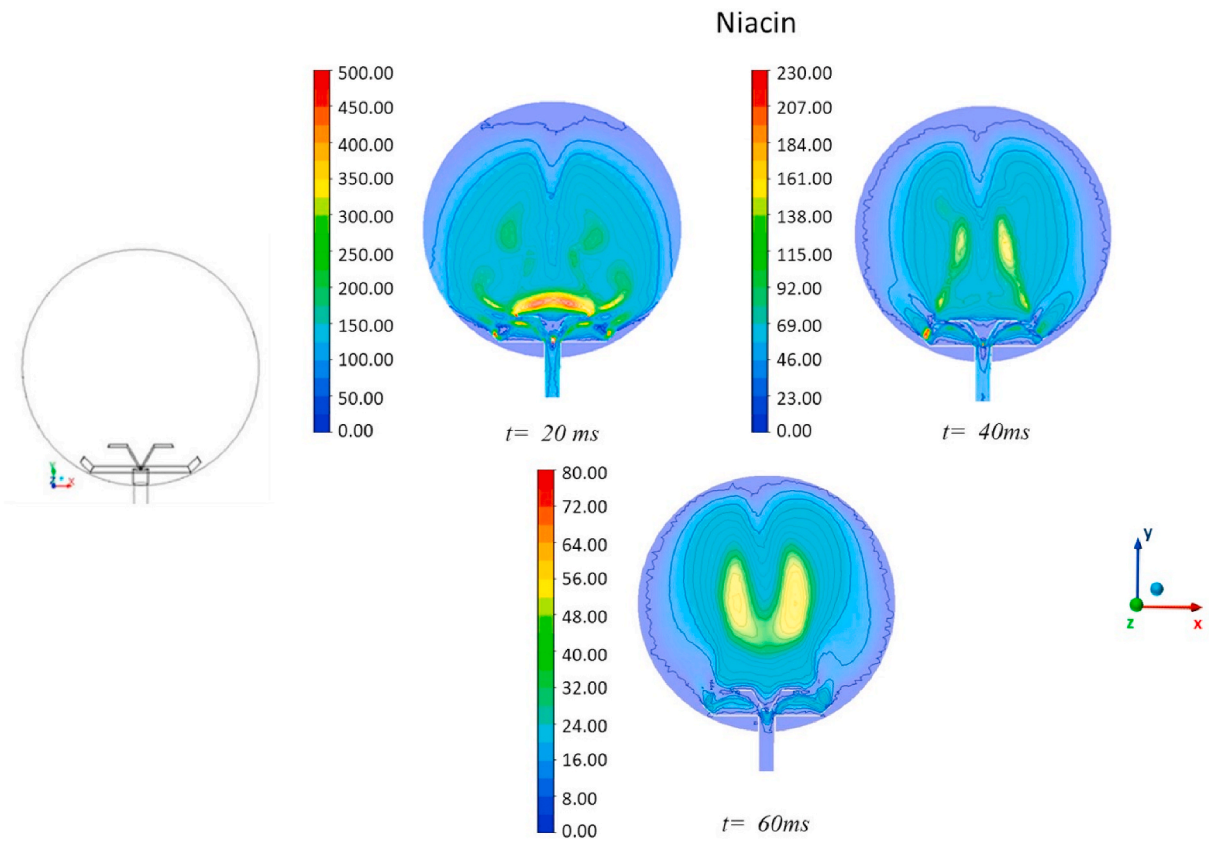

Fig. 5. Time sequence of maps of turbulence kinetic energy (m^2/s^2): niacin (frontal view).

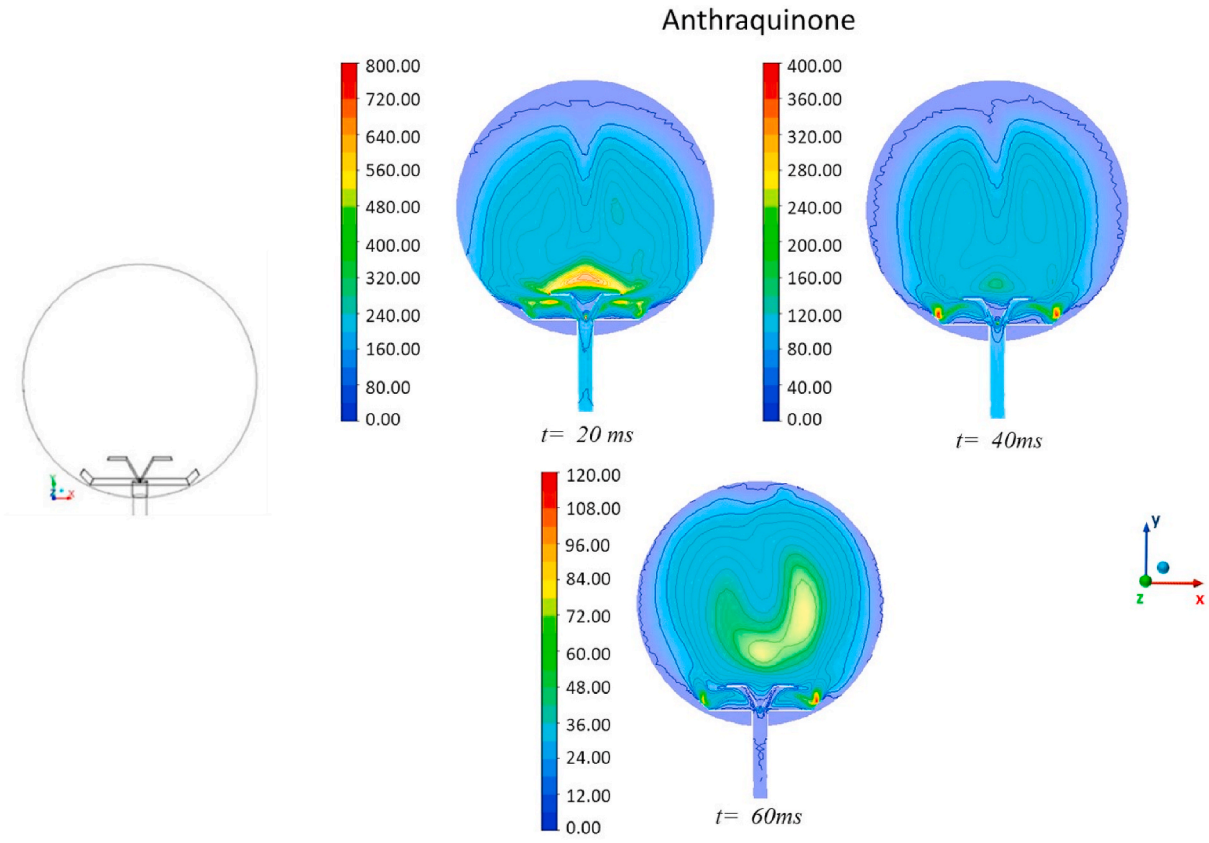

Fig. 6. Time sequence of maps of turbulence kinetic energy (m^2/s^2): anthraquinone (frontal view).

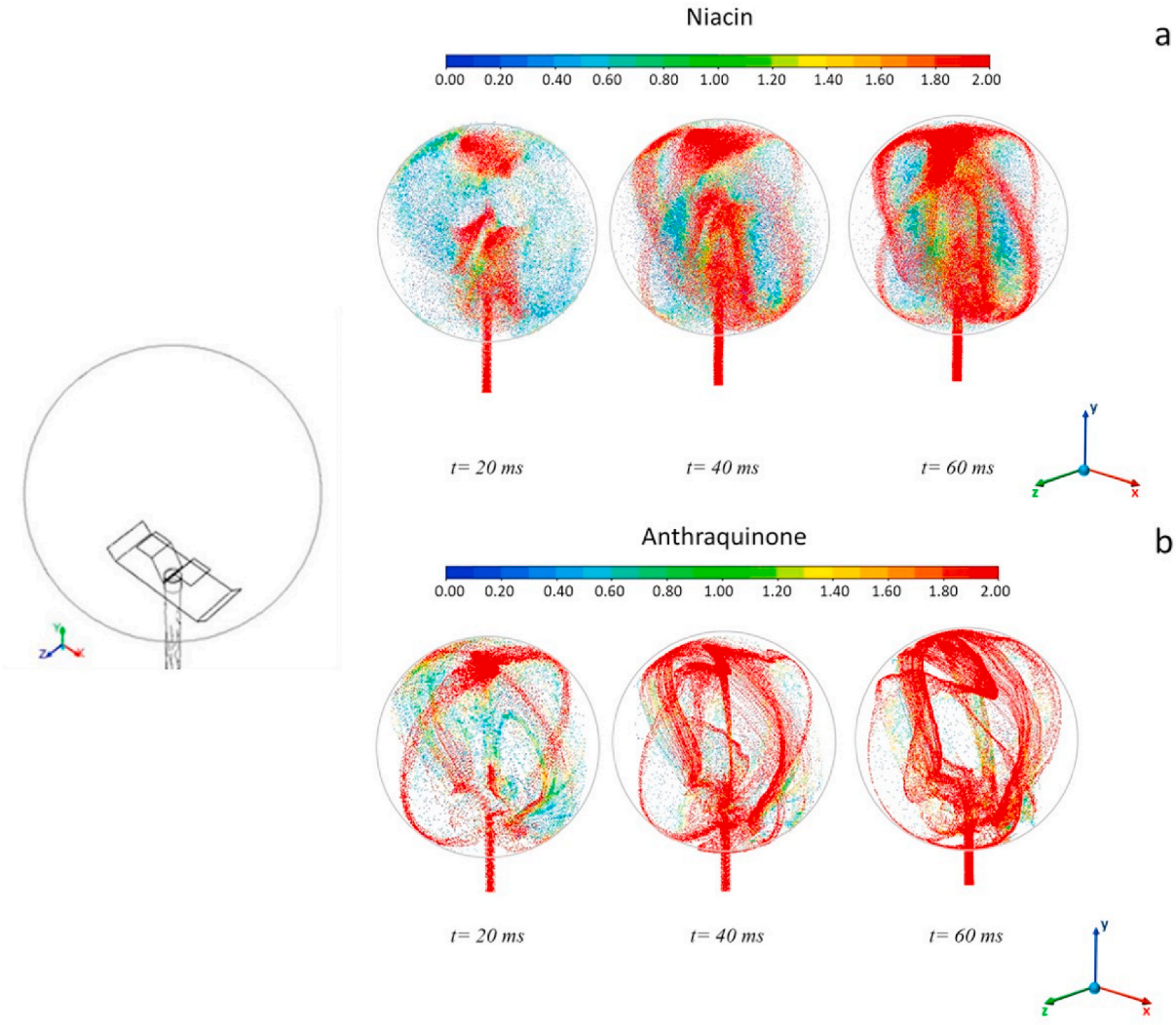

Fig. 7. Time sequence of particle tracks colored by χ (ratio between local dust concentration and nominal dust concentration) as computed for (a) niacin and (b) anthraquinone (isometric view).

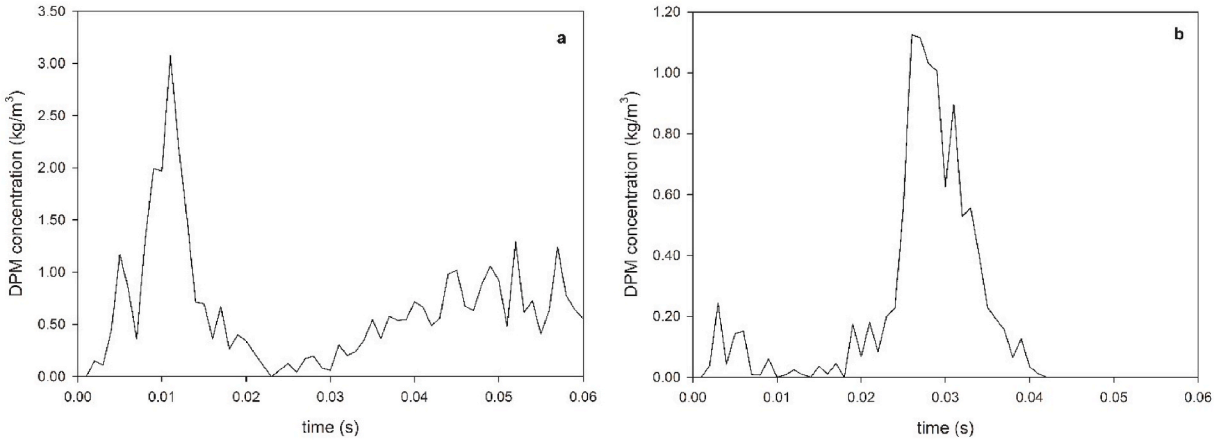

Fig. 8. DPM concentration in the center of the sphere versus time for (a) niacin and (b) anthraquinone.

($1 \cdot 10^{-4}$ s). Parallel calculations were performed by means of the segregated pressure-based solver of the code ANSYS Fluent (Release 19.0).

Simulation conditions and dust properties are given in Tables 1 and 2, respectively.

We performed simulations of mixtures of niacin and anthraquinone (25% w/w, 50% w/w, 75% w/w of niacin/total dust) to test the effects of varying particle size and density.

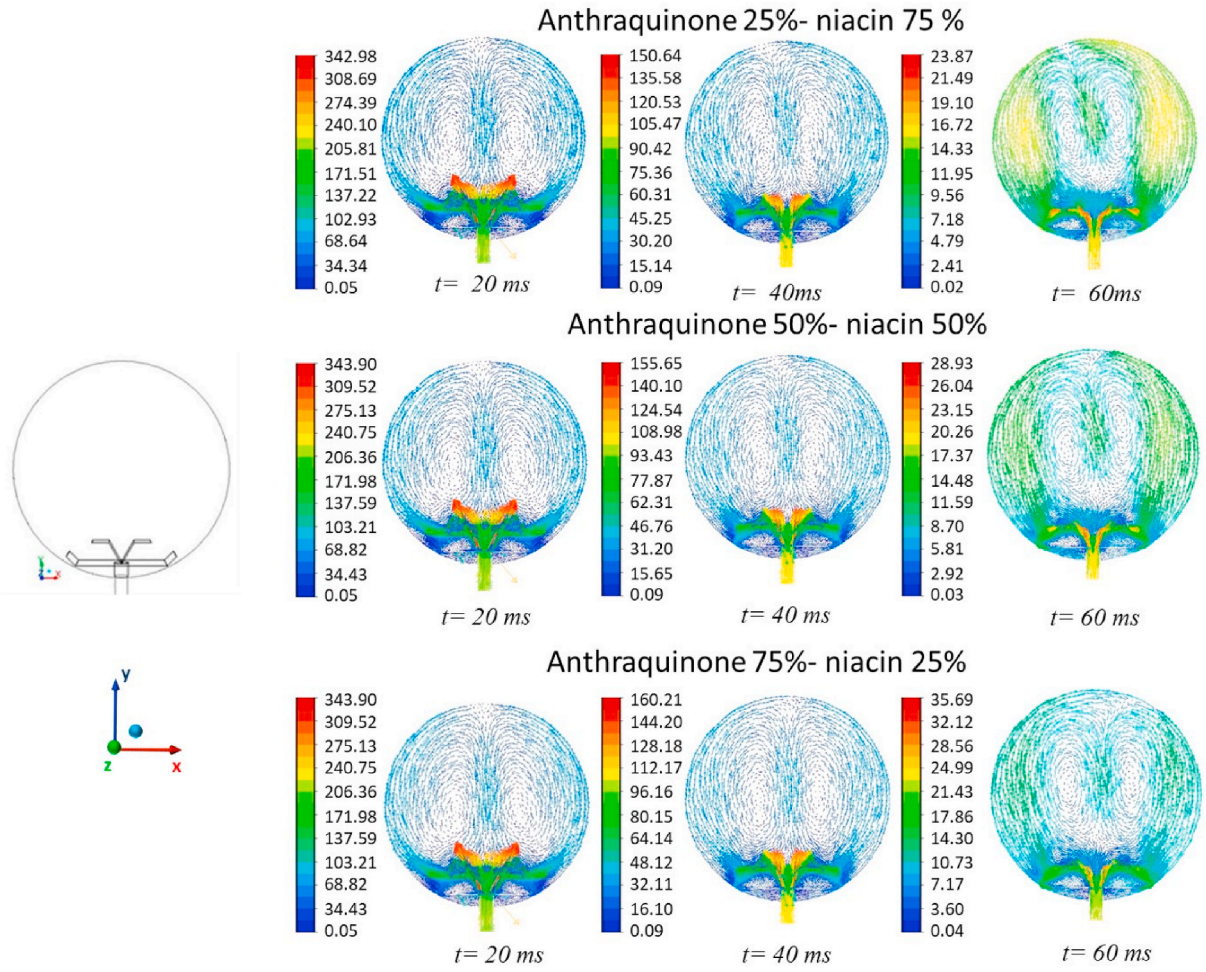

Fig. 9. Time sequences of maps of velocity vectors colored by velocity magnitude (m/s) for niacin/anthraquinone mixtures at different compositions (frontal view).

3. Results and discussion

Fig. 1 shows the pressure-time profiles as computed in the sphere and in the dust container for both niacin and anthraquinone. From these profiles, the phase during which the dust-air mixture goes from the container to the sphere (i.e., the injection phase) can be identified as a phase lasting 40 ms. Indeed, after 40 ms, the pressure in the sphere reaches 1 bar and, thus, further injection of dust-air becomes substantially negligible. Moreover, almost identical curves are simulated for both niacin and anthraquinone, meaning that the pressure-time profile is not affected by the differences in dust density and diameter.

In Fig. 1, the model results in terms of pressure-time profiles inside the sphere are compared to literature experimental data (Dahoe et al., 2002). A rather good agreement between experimental data and model predictions is found, providing a model validation. The comparison shows that, in the first 25 ms, the experimental data are slightly higher (about 11%). The simulated values need about 10 ms more to reach 1 bar. As a consequence, it is likely that, in the simulation, the dust amount that remains in the container is slightly lower.

In Fig. 2, the temporal trends of the root mean square velocity (RMS) in the case of only air, niacin and anthraquinone are shown as computed in the center of the sphere. The RMS was calculated from the turbulence kinetic energy assuming an isotropic flow field:

$$k = \frac{3}{2}(u')^2 \quad (1)$$

$$u_{RMS} = \sqrt{\overline{u'^2}} \quad (2)$$

Experimental data measured by Dahoe et al. (2002) are also shown (Dahoe et al., 2002). In particular, these are data related to both vertical and horizontal velocity component fluctuations from experiments with only air. From Fig. 2, it appears that there is a short time-period of turbulence build-up followed by a much longer time-period of turbulence decay. Turbulence starts decaying few milliseconds after the opening of the valve, well before the end of the injection phase. It is found that the RMS curves differ in the first 30 ms, while differences decrease after 30 ms. In the first part ($t < 30$ ms), the combined effects of dust concentration and dust diameter affect the spatio-temporal distribution of flow velocity and turbulence kinetic energy. Indeed, the flow development is affected not only by the dust concentration, but also by the particle size. The values of RMS for dusts are lower than the experimental values for only air. In going from anthraquinone to niacin and, thus, increasing the dust diameter, a further decrease in RMS is found.

3.1. Pure dusts

In Figs. 3 and 4, the time sequence of the maps of (flow) velocity vectors colored by the (flow) velocity magnitude is shown as computed over the frontal x-y plane of the sphere (more clearly shown in the empty images of each figure) for pure niacin and pure anthraquinone, respectively. It can be seen that vortex structures form starting from 20 ms. Such structures become well-defined at 60 ms. In both cases, asymmetric fields are simulated, especially at t = 60 ms. This behavior has also been previously found (Di Benedetto et al., 2013; Kartushinsky et al., 2011). In particular, Kartushinsky et al. (2011) developed a three-dimensional

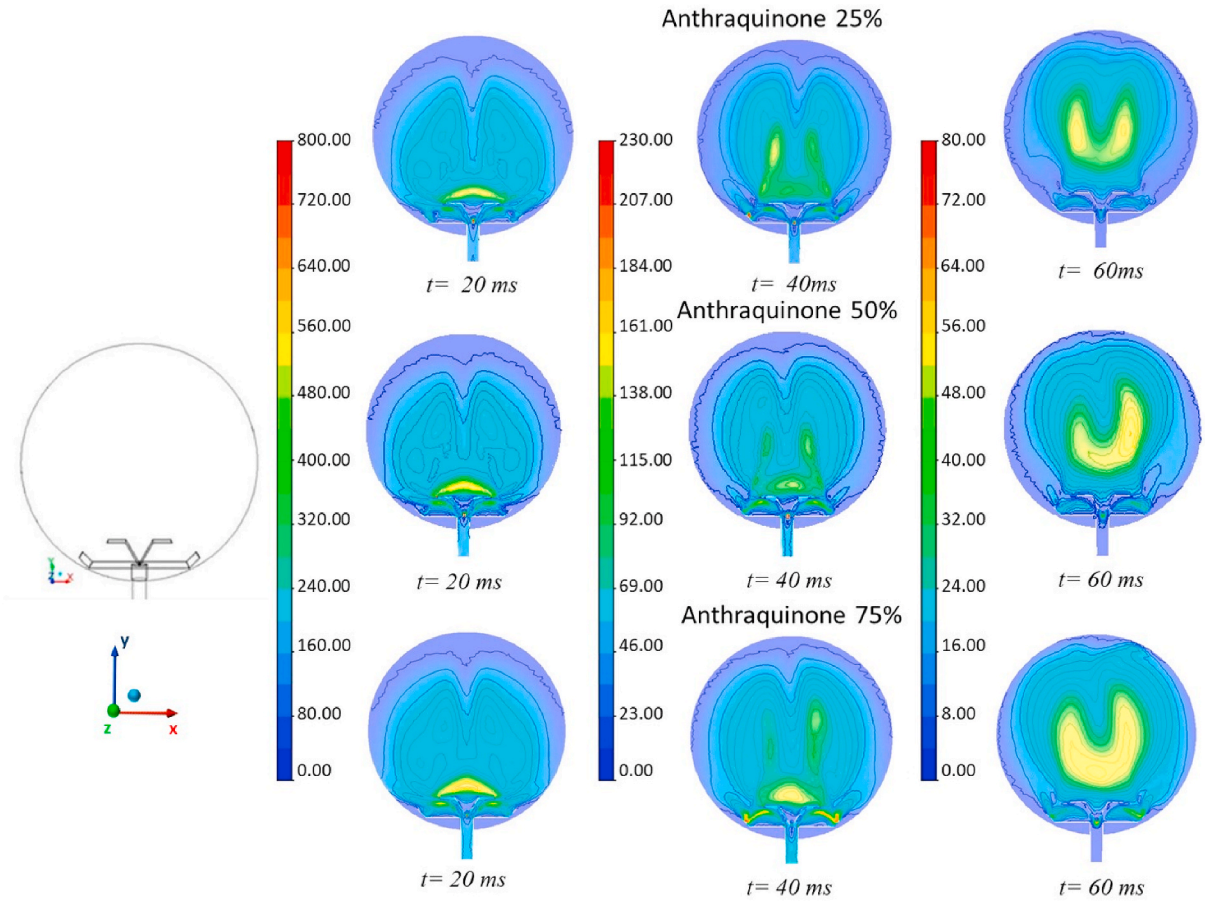

Fig. 10. Time sequences of maps of turbulence kinetic energy (m^2/s^2) for niacin/anthraquinone mixtures at different compositions (frontal view).

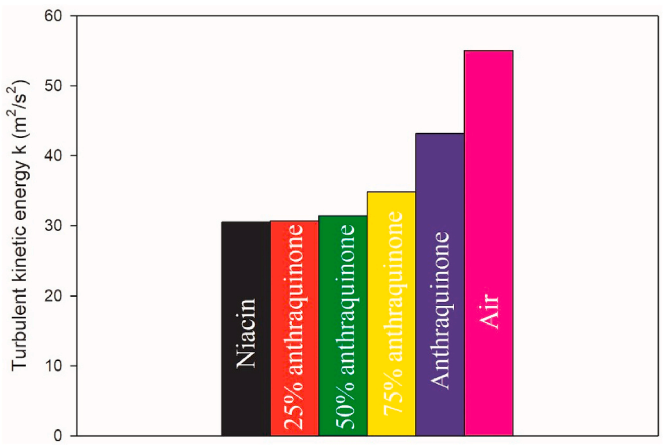

Fig. 11. Values of turbulence kinetic energy as computed in the center of the sphere at 60 ms (ignition time) for air, pure dusts, and dust mixtures at different compositions.

model of particulate flow in a horizontal pipe using the Reynolds-Averaged Navier-Stokes method. Simulation results showed that, in spite of the geometric symmetry, the presence of solid particles in the flow may return asymmetric fields due to the gravitational effect on the particles and particle sedimentation.

It is worth noting that the particle-induced asymmetry of the flow field is more evident in the case of niacin (Fig. 4), which is characterized by higher values of diameter and density than anthraquinone and, thus, by a higher value of sedimentation velocity (Stokes, 1851).

In Figs. 5 and 6, the time sequence of the maps of turbulence kinetic energy is shown as computed over the frontal x-y plane for pure niacin and pure anthraquinone, respectively. As already found for the velocity vector maps, the presence of dust gives rise to an asymmetric distribution of turbulence kinetic energy. Anthraquinone shows fields characterized by higher velocity and more intense turbulence than niacin, and this can be attributed to its smaller diameter.

The spatio-temporal distribution of dust concentration inside the sphere is shown in Fig. 7, through the time sequence of particle tracks colored by the ratio χ between the local dust concentration and the nominal dust concentration (250 g/m^3), for (a) pure niacin and (b) pure anthraquinone. Due to the presence of vortices, it appears that the highest values of dust concentration are attained close to the wall and, more generally, at the edge of the vortices. This suggests that the solid particles are not entrained by the fluid flow and, thus, the vortices represent dead volumes for the dust.

In the case of niacin (Fig. 7 (a)), the accumulation of dust particles gives rise to the formation of a three-dimensional cross, which is well evident at the ignition time (t = 60 ms). At this time, the particles are highly concentrated at the sphere wall, and values of dust concentration much higher than the nominal value are attained ($\chi = 2$; C = 500 g/m^3). This result is in agreement with the findings by Kalejaiye et al. (2010), who measured the values of transmission in different positions inside the 20 L sphere. Lower values of transmission (and, thus, higher values of concentration) were found in correspondence to the probes inside.

In the case of anthraquinone (Fig. 7 (b)), due to their smaller diameter, the dust particles are better entrained by the fluid flow and, thus, the cross-shaped structure is not predicted.

The temporal trend of dust concentration in the center of the sphere is shown in Fig. 8 for (a) niacin and (b) anthraquinone. At t = 60 ms

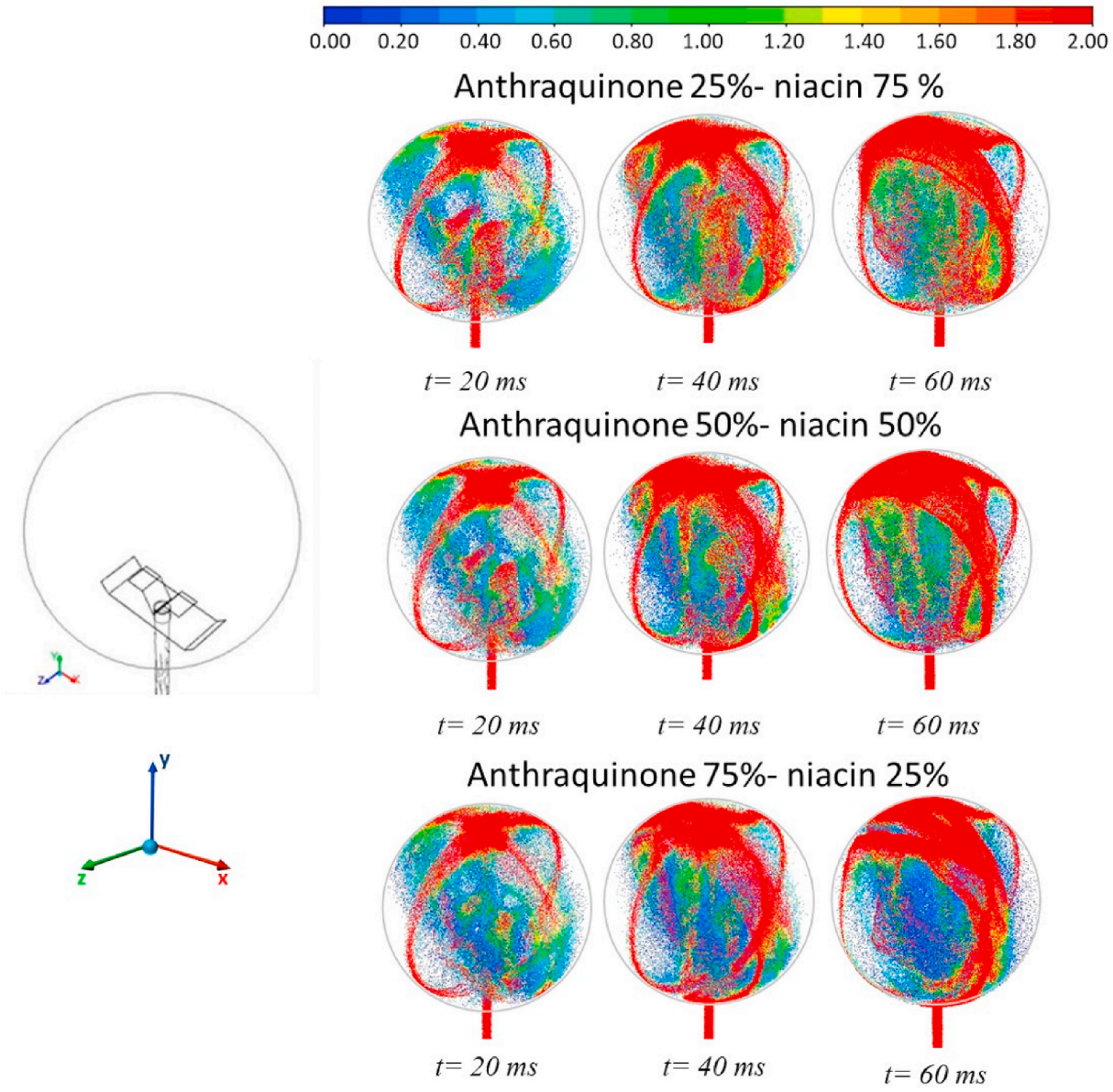

Fig. 12. Time sequences of particle tracks colored by χ (ratio between local dust concentration and nominal dust concentration) as computed for niacin/anthraquinone mixtures at different compositions (isometric view).

(ignition time), the concentration of niacin in the center is equal to 500 g/m^3, which is the same value as close to the wall. This is a result of the fact that niacin particles are located mainly at the edge of the vortices. Conversely, at t = 60 ms, the concentration of anthraquinone in the center is equal to zero. In this case, beyond diameter, density plays a role. The higher the density ratio between dust and gaseous medium, the lower the capability of the vortices to entrain the solid particles. Niacin is more dense than anthraquinone and, thus, niacin particles are concentrated mainly at the edge of the vortices (Vigolo et al., 2014), while anthraquinone is dispersed in the internal zone of the vortices. For both the pure dusts, the value of concentration in the center at the ignition time differs from the nominal value, and the distribution of particles is strongly non-uniform.

3.2. Dust mixtures

In Fig. 9, the time sequences of the maps of (flow) velocity vectors colored by the (flow) velocity magnitude are shown as computed over the frontal x-y plane of the sphere (more clearly shown in the empty images of each figure) for niacin/anthraquinone mixtures at different compositions. As in the case of pure dusts, due to the presence of vortices, the highest values of dust concentration are attained close to the wall and, thus, in zones external to the vortices themselves. This suggests that the solid particles are not entrained by the fluid flow and, thus, the vortices are dead volumes for the dust.

In Fig. 10, the time sequences of the maps of turbulence kinetic energy are shown as computed over the frontal x-y plane for niacin/anthraquinone mixtures at different compositions. Even in the case of dust mixtures, an asymmetric distribution of turbulence kinetic energy is simulated. As discussed in Section 3.1., due to the smaller particle diameter, anthraquinone shows fields characterized by higher velocity and more intense turbulence than nicotinic acid. Thus, as the concentration of anthraquinone in the dust mixture is increased, the turbulence kinetic energy increases. This is confirmed by Fig. 11 showing the values of turbulence kinetic energy in the center of the sphere at 60 ms (ignition time) for air, pure dusts, and dust mixtures at different compositions. This figure clearly shows the trend of increasing turbulence kinetic energy with increasing concentration of anthraquinone in the dust mixture

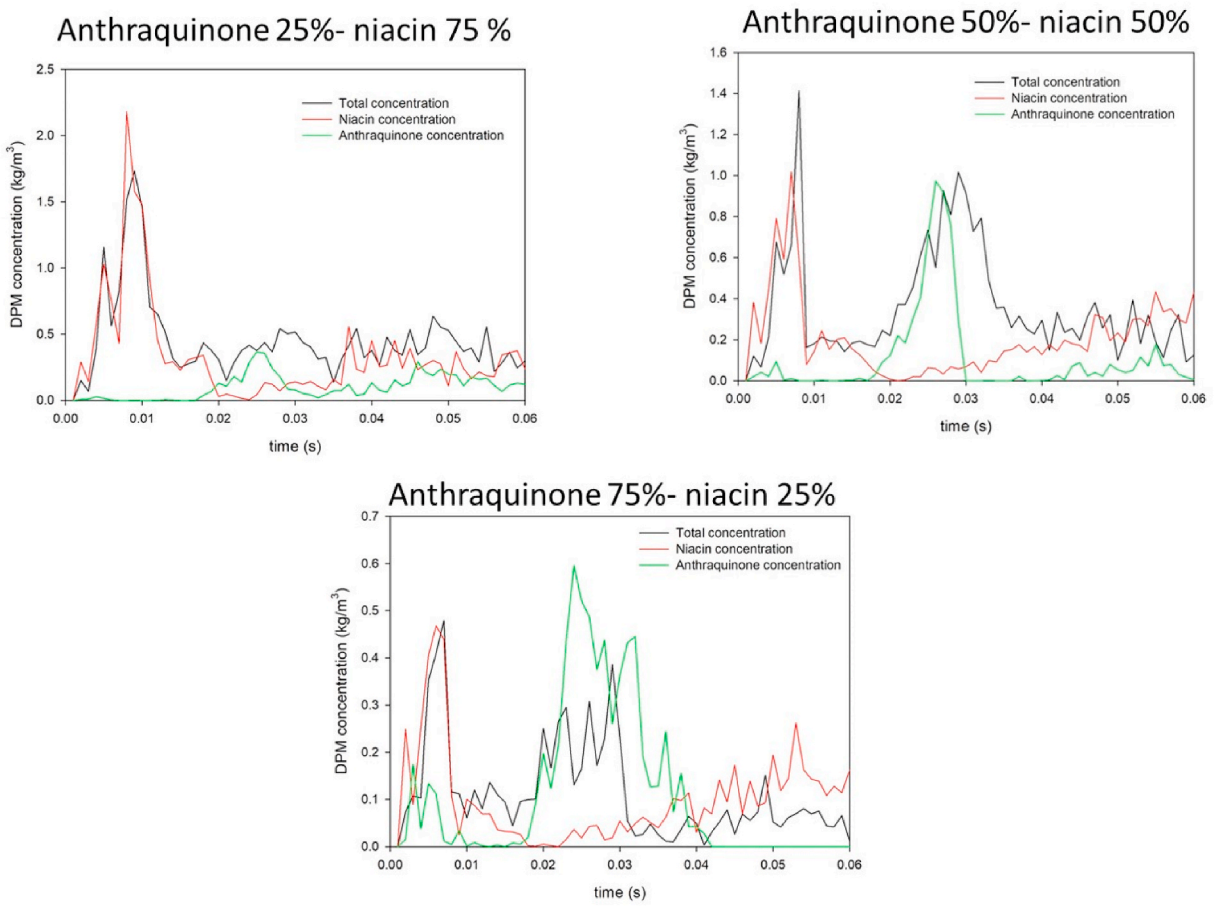

Fig. 13. DPM concentrations in the center of the sphere versus time for niacin/anthraquinone mixtures at different compositions.

(i.e., in going from pure niacin to pure anthraquinone). However, the highest value of turbulence kinetic energy is attained in the case of air without dust.

The spatio-temporal distribution of dust concentration inside the sphere is shown in Fig. 12, through the time sequences of particle tracks colored by the ratio χ between the local dust concentration and the nominal dust concentration (250 g/m^3), for dust mixtures at different compositions. This figure further confirms that the highest values of dust concentration are attained externally to the vortices. In particular, at the ignition time (t = 60 ms), the dust is highly concentrated at the sphere wall, and values of concentration higher than the nominal value are predicted (χ = 2; C = 500 g/m^3). Due to the higher ability of anthraquinone to be entrained by the fluid flow, the internal zone of the vortices is gradually filled by solid particles with increasing concentration of anthraquinone in the dust mixture.

The temporal trend of dust concentration in the center of the sphere is shown in Fig. 13 for niacin/anthraquinone mixtures at different compositions. In particular, for each mixture composition, the temporal trends of total concentration and concentration of the two pure dusts are plotted. The total concentration is always different from the nominal one and, at the ignition time (t = 60 ms), only niacin is present at the center of the sphere. As a consequence, in the case of spark ignition, it is likely that only niacin will be ignited, anthraquinone concentration being almost zero. In the case of chemical igniters, due to the larger ignition volume, also anthraquinone will be involved in ignition. However, regardless of the ignition type, the strongly non-uniform dust distribution affects the flame speed and, then, the pressure rise.

Global assessment of the results obtained for dust mixtures, thus, demonstrates that a new issue arises. Since pure dusts may have quite different properties (diameter, density, shape, etc.), in the case of dust mixtures, particles will follow preferential paths that are dictated by these differences, thus resulting in zones richer in a pure constituent and poorer in the other one and *vice versa*. This issue is further confirmed by Fig. 14 showing the particle tracks colored by (normalized) total and pure dust concentrations as computed at the ignition time for niacin/anthraquinone mixtures at different compositions. Due to the different properties, pure dusts are not homogenously mixed up within the sphere but, on the contrary, they tend to segregate. This issue negatively affects repeatability and reliability of experimental tests carried out in the standard 20 L sphere to evaluate safety parameters of dust mixtures.

4. Conclusions

A validated three-dimensional CFD model was used to simulate the dust dispersion inside the 20 L sphere for niacin/anthraquinone mixtures at different compositions (i.e., pure dust ratios, while keeping the total dust concentration constant). Simulations for pure dusts were also performed.

In the case of pure dusts, the time sequences of velocity vector maps show that multiple vortex structures are established inside the sphere, generating dead volumes for the solid particles, which are pushed towards the edges of the vortices. This is especially true for niacin. Due to its lower diameter and density, anthraquinone can be better entrained by the fluid flow. However, for each pure dust, the value of concentration in the center of the sphere at the ignition time (60 ms) differs from the nominal value.

In the case of dust mixtures, the dispersion inside the sphere is strongly non-uniform, with zones richer in niacin and poorer in anthraquinone and *vice versa*.

Overall, the obtained results demonstrate that, to perform a correct

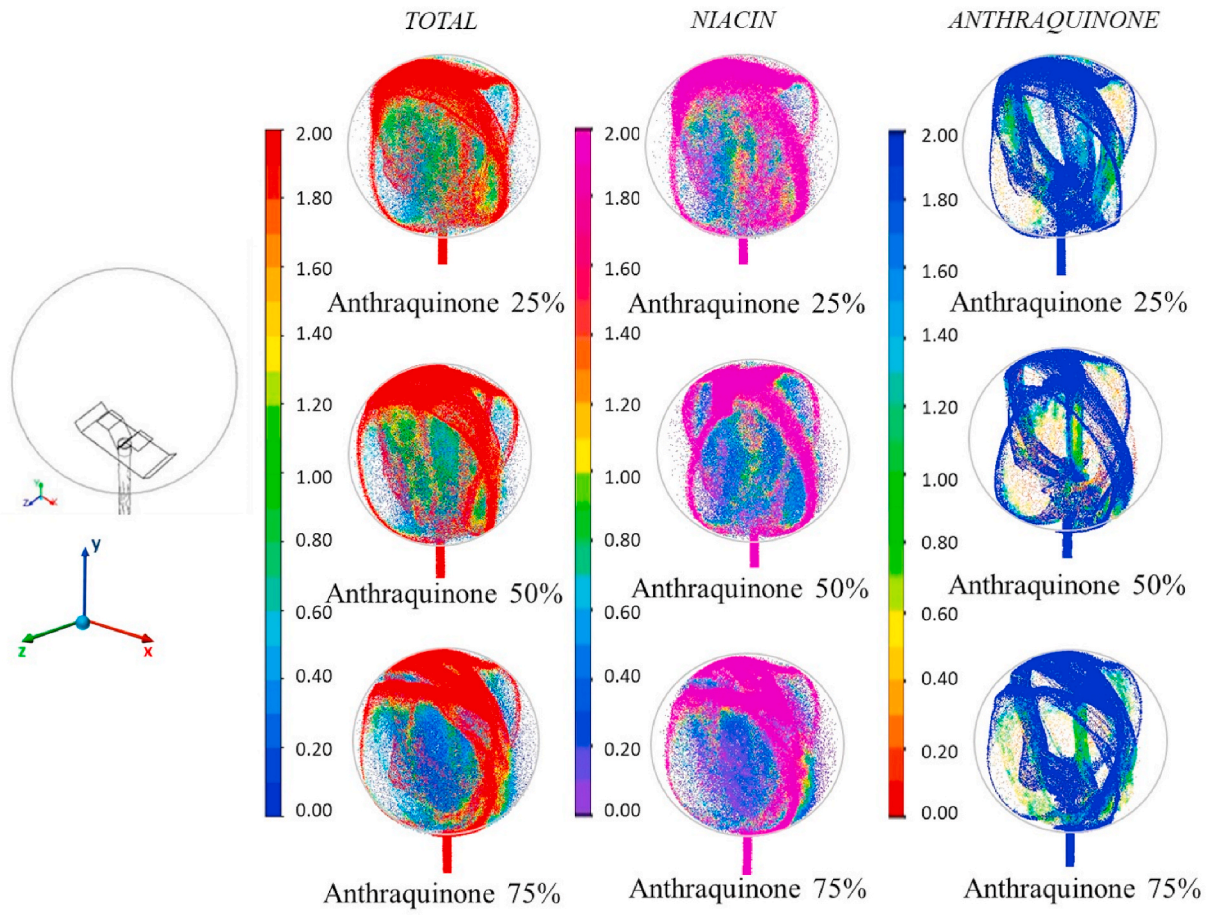

Fig. 14. Particle tracks colored by (normalized) total and pure dust concentrations as computed at 60 ms (ignition time) for niacin/anthraquinone mixtures at different compositions (isometric view).

and reliable evaluation of flammability and explosibility parameters for dusts and dust mixtures, a different dispersion method has to be developed. When testing dust mixtures, this is needed not only to guarantee a uniform dispersion of the solid particles, but to also ensure the nominal mixture composition in each point of the sphere.

Author contributions

Maria Portarapillo: Methodology; Investigation; Writing - original draft; Writing - Review & Editing. **Valeria Di Sarli:** Resources; Writing - Review & Editing. **Roberto Sanchirico:** Investigation; Writing - Review & Editing. **Almerinda Di Benedetto:** Conceptualization; Resources; Writing - original draft; Writing - Review & Editing; Supervision.

Declaration of competing interest

The authors declare that they have no known competing financial interests or personal relationships that could have appeared to influence the work reported in this paper.

References

ASTM E1226-19, 2019. Standard Test Method for Explosibility of Dust Clouds. ASTM Int., West Conshohocken, PA, pp. 1–15.
ASTM E1491-06, 1991. Standard Test Method for Minimum Autoignition Temperature of Dust Clouds. ASTM Int., West Conshohocken, PA, pp. 1–10.
ASTM E1515-14, 1993. Standard Test Method for Minimum Explosible Concentration of Combustible Dusts 1. ASTM Int., West Conshohocken, PA, pp. 1–9.
ASTM E2019-03, 1999. Standard Test Method for Minimum Ignition Energy of a Dust Cloud in Air. ASTM Int., West Conshohocken, PA, pp. 1–9.
ASTM E2021-15, 1999. Standard Test Method for Hot-Surface Ignition Temperature of Dust Layers. ASTM Int., West Conshohocken, PA, pp. 1–10.
ASTM E2931-13, 2013. Standard Test Method for Limiting Oxygen (Oxidant) Concentration of Combustible. ASTM Int., West Conshohocken, PA, pp. 1–9.
ASTM E502-07, 1984. Standard Test Method for Selection and Use of ASTM Standards for the Determination of Flash Point of Chemicals by Closed Cup Methods. ASTM Int., West Conshohocken, PA, pp. 1–6. https://doi.org/10.1520/E0502-07E01.priate.
Centrella, L., Portarapillo, M., Luciani, G., Sanchirico, R., Di Benedetto, A., 2020. Synergistic behavior of flammable dust mixtures: a novel classification. J. Hazard Mater. 397 https://doi.org/10.1016/j.jhazmat.2020.122784.
Dahoe, A.E., Cant, R.S., Scarlett, B., 2002. On the decay of turbulence in the 20-liter explosion sphere. Flow, Turbul. Combust. 67, 159–184. https://doi.org/10.1023/A:1015099110942.
Di Benedetto, A., Russo, P., Amyotte, P., Marchand, N., 2010. Modelling the effect of particle size on dust explosions. Chem. Eng. Sci. 65, 772–779. https://doi.org/10.1016/j.ces.2009.09.029.
Di Benedetto, A., Russo, P., Sanchirico, R., Di Sarli, V., 2015. A fan-equipped reactor for dust explosion tests. AIChE 61, 1572–1580. https://doi.org/10.1002/aic.
Di Benedetto, A., Russo, P., Sanchirico, R., Di Sarli, V., 2013. CFD simulations of turbulent fluid flow and dust dispersion in the 20 liter explosion vessel. AIChE 59, 2485–2496. https://doi.org/10.1002/aic.
Di Sarli, V., Russo, P., Sanchirico, R., Di Benedetto, A., 2014. CFD simulations of dust dispersion in the 20 L vessel: effect of nominal dust concentration. J. Loss Prev. Process. Ind. 27, 8–12. https://doi.org/10.1016/j.jlp.2013.10.015.
Di Sarli, V., Russo, P., Sanchirico, R., Di Benedetto, A., 2013. CFD simulations of the effect of dust diameter on the dispersion in the 20L bomb. Chem. Eng. Trans. 31, 727–732.
Di Sarli, V., Sanchirico, R., Russo, P., Di Benedetto, A., 2015. CFD modeling and simulation of turbulent fluid flow and dust dispersion in the 20-L explosion vessel equipped with the perforated annular nozzle. J. Loss Prev. Process. Ind. 38, 204–213. https://doi.org/10.1016/j.jlp.2015.09.015.
Elghobashi, S., 1994. On predicting particle-laden turbulent flows. Appl. Sci. Res. 52, 309–329. https://doi.org/10.1007/BF00936835.
Hauert, F., Vogl, A., 1995. Measurement of Dust Cloud Characteristics in Industrial Plants.

Kalejaiye, O., Amyotte, P.R., Pegg, M.J., Cashdollar, K.L., 2010. Effectiveness of dust dispersion in the 20-L Siwek chamber. J. Loss Prev. Process. Ind. 23, 46–59. https://doi.org/10.1016/j.jlp.2009.05.008.

Kartushinsky, A.I., Michaelides, E.E., Rudi, Y.A., Tisler, S.V., Shcheglov, I.N., 2011. Numerical simulation of three-dimensional gas-solid particle flow in a horizontal pipe. AIChE J. 57, 2977–2988. https://doi.org/10.1002/aic.12528.

Launder, B.E., Spalding, D.B., 1972. Lectures in Mathematical Models of Turbulence. Academic Press, London; New York.

Portarapillo, M., Luciani, G., Sanchirico, R., Di Benedetto, A., 2020. Ignition mechanism of flammable dust and dust mixtures: an insight through TG/DSC analysis. AIChE J. https://doi.org/10.1002/aic.16256.

Pu, Y.K., Jarosinski, J., Johnson, V.G., Kauffman, C.W., 1991. Turbulence effects on dust explosions in the 20-liter spherical vessel. Symp. Combust. 23, 843–849. https://doi.org/10.1016/S0082-0784(06)80338-3.

Russo, P., Amyotte, P.R., Khan, F.I., Di Benedetto, A., 2013. Modelling of the effect of size on flocculent dust explosions. J. Loss Prev. Process. Ind. 26, 1634–1638. https://doi.org/10.1016/j.jlp.2013.07.012.

Russo, P., Di Benedetto, A., 2013. Review of a dust explosion modeling. Chem. Eng. Trans. 31, 955–960. https://doi.org/10.3303/CET1331160.

Sanchirico, R., Di Sarli, V., Di Benedetto, A., 2018. Volatile point of dust mixtures and hybrid mixtures. J. Loss Prev. Process. Ind. 56, 370–377. https://doi.org/10.1016/j.jlp.2018.09.014.

Sanchirico, R., Di Sarli, V., Russo, P., Di Benedetto, A., 2015a. Effect of the nozzle type on the integrity of dust particles in standard explosion tests. Powder Technol. 279, 203–208. https://doi.org/10.1016/j.powtec.2015.04.003.

Sanchirico, R., Russo, P., Di Sarli, V., Di Benedetto, A., 2015b. On the explosion and flammability behavior of mixtures of combustible dusts. Process Saf. Environ. Protect. 94, 410–419. https://doi.org/10.1016/j.psep.2014.09.007.

Stokes, G.G., 1851. On the effect of the internal friction of fluids on the motion of pendulums. Trans. Cambridge Philos. Soc. 9, 1–86. https://doi.org/10.1017/cbo9780511702266.002.

van der Wel, P.G.J., van Veen, J.P.W., Lemkowitz, S.M., Scarlett, B., van Wingerden, C.J. M., 1992. An interpretation of dust explosion phenomena on the basis of time scales. Powder Technol. 71, 207–215. https://doi.org/10.1016/0032-5910(92)80010-T.

Vigolo, D., Radl, S., Stone, H.A., 2014. Unexpected trapping of particles at a T junction-Supporting Information. Proc. Natl. Acad. Sci. U.S.A. 111, 1–15.

Zalosh, R., 2019. Dust explosions: regulations, standards, and guidelines. In: Methods in Chemical Process Safety, first ed. Elsevier Inc. https://doi.org/10.1016/bs.mcps.2019.03.003.